



A small-footprint Cavity Ring-Down Spectroscopy instrument for in-situ measurements of NO₃ and N₂O₅

Gunther N. T. E. Türk^{1*}, Simone T. Andersen¹, Patrick Dewald¹, Jan Schuladen¹, Jos Lelieveld¹ and John N. Crowley^{1*}

5 ¹Atmospheric Chemistry Department, Max Planck Institute for Chemistry, 55128 Mainz, Germany

*Correspondence to: Gunther N. T. E. Türk (g.tuerk@mpic.de) and John N. Crowley (john.crowley@mpic.de)

Abstract.

We present a new, small-footprint instrument for point measurements of NO₃ and N₂O₅. Both molecules play an important role in nocturnal atmospheric chemistry, impacting the NO_x-budget and the oxidation of biogenic volatile organic compounds. NO₃ and N₂O₅ are often present at concentrations of a few parts per trillion by volume (pptv) and their measurements in remote locations requires instrumentation that is easily transported and lightweight, but maintains high sensitivity and accuracy. We have constructed a relatively compact and light instrument for Cavity Ring-Down Spectroscopy (CRDS) with the dimensions (width × depth × height) of 55 × 55 × 150 cm and a weight of 50 kg that uses two independent cavities to quantify the mixing ratio of NO₃ using an inlet at room temperature and the sum of NO₃ + N₂O₅ via a thermal dissociation inlet. Under laboratory conditions, limits of detection (1σ Allan deviation at 1 s integration) for the NO₃ and (NO₃ + N₂O₅) channel are < 1 pptv and < 2 pptv, respectively. This improves to about 0.1 pptv and 0.2 pptv for 3-minute integration. The total measurement uncertainty for NO₃ is 9.8 % and ≥ 11.5 % for N₂O₅, depending on the NO₃-to-N₂O₅ ratio. In this publication, we present design details of the instrument, discuss its performance in a controlled environment as well as during a field campaign. Additionally, we present measurements of transmission losses for NO₃ across different filter types and methods to reduce filter reactivity and allow reusability after a cleaning procedure.

1 Introduction

The nitrate radical (NO₃) and dinitrogen pentoxide (N₂O₅) are important trace gases for nocturnal chemistry (Wayne et al., 1991). NO₃ serves as a key nighttime initiator of nocturnal oxidation and, through its reactions with biogenic trace gases, plays an important role in linking anthropogenic and biogenic emissions (Ng et al., 2017). Originating predominantly from combustion-related anthropogenic sources, nitrogen oxides (NO_x = NO + NO₂) can be oxidized by ozone (O₃) resulting in the formation of NO₃ via Reactions (R1) and (R2).





NO₃ is photolabile and reacts rapidly with NO (R3) so that NO₃ mixing ratios exceed a few pptv (parts per trillion by volume) only at nighttime (Brown et al., 2003). The major nocturnal losses of NO₃ are reaction with unsaturated (often biogenic) hydrocarbons like monoterpenes (R4), especially in forested regions (Atkinson and Arey, 2003). As the lifetime of NO at night is short (owing to reaction with O₃) it contributes to NO₃ nocturnal losses only when locally emitted from either combustion sources or soil (Pilegaard, 2013).



The organic nitrate products from reaction (R4) at nighttime can contribute to secondary organic aerosol, be lost via dry deposition or hydrolysis to HNO₃ or be photolysed the next day (Ng et al., 2017). The termolecular association reaction of NO₃ with NO₂ generates N₂O₅ (R5), which, through its thermal decomposition (R6), exists in thermal equilibrium with NO₃ and NO₂. In the boundary layer of temperate regions, all three constituents can coexist in detectable amounts.



The thermal equilibrium is described by the equilibrium constant $K_{eq} = k_5/k_6$ with the respective rate coefficients k_i associated with reaction (Ri). N₂O₅ can undergo heterogeneous hydrolysis to form aqueous HNO₃ on particles, which can then be removed from the atmosphere by wet or dry deposition. NO₃ and N₂O₅ can thus be considered intermediates in NO_x loss at night and thereby reduce the rate of production of O₃ the following day (Finlayson-Pitts and Pitts, 2000). Understanding their behaviour is necessary to improve our understanding of chemistry within the nocturnal boundary layer.

NO₃ has a strong absorption feature at ~ 662 nm which has been used to detect NO₃ using Differential Optical Absorption Spectroscopy (DOAS) over long path lengths using natural light sources such as moon-light (Noxon et al., 1978; Smith and Solomon, 1990; Wagner et al., 2000), scattered sunlight (Aliwell and Jones, 1998; Allan et al., 2002; Von Friedeburg et al., 2002; Geyer et al., 2003) and artificial light sources for “active” DOAS measurements of NO₃ close to ground level over path lengths of a few km (Platt et al., 1980; Geyer et al., 2001; Smith et al., 1995; Carslaw et al., 1997; Stutz et al., 2004). Note that DOAS instruments do not detect N₂O₅.

The availability of highly reflective cavity mirrors and cheap laser diodes has recently resulted in a great increase in the deployment of optical resonator (“cavity”) instruments in which two highly reflective mirrors are used to generate effective absorption path lengths of several tens of kilometres (Mazurenka et al., 2005; Berden et al., 2000). Cavity enhanced absorption spectroscopy (CEAS) and cavity ring-down spectroscopy (CRDS) (Brown and Stutz, 2012) typically attain very low and sub-pptv limits of detection (Dorn et al., 2013) and have become the most common methods for measuring NO₃. The detection of N₂O₅ (via cavity spectroscopy or laser induced fluorescence (LIF)) is achieved via its conversion (in a “thermal dissociation inlet”) to NO₃ so that the sum of both ambient NO₃ and thermally dissociated N₂O₅ is measured (Brown et al., 2001; Ayers et al., 2005; Schuster et al., 2009; Matsumoto et al., 2005). Similar to absorption spectroscopy methods based on the Lambert-Beer law, CEAS and CRDS require “zero” measurements without absorbing gaseous species (i.e., NO₃), which can be achieved by flowing synthetic air through the instrument or the addition of NO to the inlet, which converts NO₃ to NO₂ (R3).



During field campaigns, compact and transportable instruments offer significant advantages, especially for remote (Ayers and Simpson, 2006), elevated (Brown et al., 2007), or airborne measurements (Dubé et al., 2006). In this paper, we present a new
65 “small-footprint”, 2-channel CRDS instrument (“2CH-CRDS”) for ambient measurements of NO₃ and N₂O₅. We describe the operational principles, its design and the results from laboratory characterization measurements as well as its performance during field campaigns.

2 The Instrument – Cavity Ring-Down Spectroscopy

CRDS is a direct absorption measurement technique with high sensitivity. CRDS requires a light source, a high-finesse cavity
70 and a detector that records the intensity of transmitted light exiting the cavity. To determine the mixing ratio of NO₃ ([NO₃]), the exponential decay of the measured light intensity, also called “ring-down”, is recorded after switching off the light source. The corresponding time constant τ (“ring-down time constant”) depends on the mirror reflectivity and the distance between the mirrors and is reduced in the presence of an absorber within the cavity. The mixing ratio of NO₃ can be calculated by Equation (1).

$$75 \quad [\text{NO}_3] = \frac{R_L}{c \cdot \sigma} \cdot \left(\frac{1}{\tau} - \frac{1}{\tau_0} \right) \quad (1)$$

Here, τ is measured in the presence of NO₃ and τ_0 ($> \tau$) in the absence of NO₃ which is typically achieved by the addition of NO to titrate NO₃ via R3. Furthermore, c denotes the speed of light, σ is the effective absorption cross-section of NO₃ for the laser emission spectrum and R_L (≥ 1) is the ratio between the mirror distance and the actual absorption path length inside the cavity. For most instruments R_L is greater than 1, because a flow of clean air is used to protect the mirrors from contamination
80 (see Section 3.2). The sensitivity of this method depends on the minimal detectable difference in ring-down times $\Delta\tau_{min} = \lim_{\tau \rightarrow \tau_0} (\tau_0 - \tau)$ and the theoretical limit of detection (LOD) is given by Equation (2).

$$\text{LOD} = \frac{R_L}{c \cdot \sigma} \cdot \frac{\Delta\tau_{min}}{\tau_0^2} \quad (2)$$

This highlights the importance of precise τ measurements with very low variation and therefore requires stable mirror alignment. In practice, the LOD has to be determined for a certain measurement period and is affected by e.g. temperature
85 drifts (hence thermal insulation of the cavities) and changes in air mass composition (e.g. water content) which are the reason for zero measurements every few minutes.

For this instrument, both cavities are defined by two concave mirrors (1 m focal length, $R > 0.99998$ at 662 nm, FiveNine Optics) separated by a distance (d) of about 74 cm, which results in an effective absorption pathlength of approximately 37 km
90 ($= d/(1 - R)$). The planar outer face of the mirrors is anti-reflection coated to minimize initial losses of laser intensity. For this instrument, typical ring-down times range from 140 μs to 170 μs , which is comparable to those from similarly designed instruments operating at near-ambient pressure (Sobanski et al., 2016; Dubé et al., 2006; Ayers et al., 2005; Brown et al., 2002). The ring-down times depend strongly on the adjustment and the cleanliness of the mirrors. A new mirror mount design



is presented in the following section, while for cleaning the mirrors, we found that using ESD-free First Contact Polymer solution (Photonic Cleaning Technologies) is more reliable in restoring high reflectivity than the standard application of acetone or isopropanol, especially under field conditions.

2.1 Instrument design

Our 2CH-CRDS instrument is installed in an aluminium profile rack ($\sim 55 \times 55 \times 150$ cm), weighs approximately 50 kg and uses two almost identical channels (where the term “channel” means cavity plus associated inlets) to measure NO_3 as well as $\text{NO}_3 + \text{N}_2\text{O}_5$ after thermal dissociation (TD) of N_2O_5 . The instrument is illustrated in Figure 1. Both channels are vertically aligned and accessible from the front of the instrument for adjusting the cavity mirrors. The cavities are insulated with custom-made heating / insulation sleeves (HORST GmbH) that match the T-shape geometry (arm lengths of 2×30 cm and 1×25 cm) of the glass tubing (1/2-inch outer diameter, 9 mm inner diameter). While the shorter arm is used as an entrance, the longer arms define most of the absorption path length. The inner walls are coated with Teflon (FEPD-121, Chemours) to reduce wall losses of NO_3 (more details will be given in Section 3.6).

With the left-hand cavity, we detect NO_3 at room temperature. In the channel on the right-hand side, the absorption path is maintained at 105°C (outer glass wall temperature), with its TD inlet held at 170°C to convert all N_2O_5 into NO_3 . Together, this results in a gas temperature of 100°C along the absorption path. All temperature read-and-control units (diraView and Quantrol series, Jumo GmbH) are operated with standard PT1000 sensors (RS PRO). The rear side of the instrument houses a laboratory power supply, mass flow controllers (MFCs), an automatic filter changer and all electronics required for data acquisition.

2.2 Air Flow

The flow of air through the instrument is depicted by black arrows in Figure 1. Unless otherwise stated, we use 1/4-inch PFA tubing and PFA fittings (Swagelok) for all connections. Air enters the instrument via an automatic filter changer (modified from Sobanski et al. (2016) and similar to that described by Dubé et al. (2006)) and PTFE filters, which prevent particles from contaminating the instrument. Directly underneath the filter changer, NO for zero measurements (titration of NO_3 , R3) is added via a T-piece. Similar to Schuster et al. (2009), we use two MFCs (IQF-200C, Bronkhorst GmbH) and 1/8-inch PFA tubing to reduce the switching time between ambient and zero measurements. The first MFC continuously flows 7 standard (STP) cubic centimetres per minute (sccm) of NO (200 parts per million by volume (ppmv) in N_2 , Air Liquide) while the second MFC (set to 9 sccm) is connected to a solenoid valve and an exhaust system. During zero measurements, the solenoid valve is closed and NO is added to the sampled ambient air. Opening the valve directs the NO (plus 2 sccm of sampled air) to the exhaust, allowing NO_3 and N_2O_5 to be measured. This setup results in a switching time of ~ 2 seconds (depending on the flow of sampled air) and zero measurements are performed every 3 minutes for 10–15 seconds.

Following the NO addition point, the sampled ambient air is split into both channels, each regulated by a MFC (FG-201CV, Bronkhorst) set to 7200 sccm. The major contribution of this total flow is 7000 sccm sampled air, which again splits into two



125 directions, with flows of 3500 sccm towards each cavity mirror. The cavity mirrors are protected against contamination by a
200 sccm “counter” flow of purge gas (light-blue arrows, clean dry air, IQF-200C, Bronkhorst GmbH), which mixes with the
sampled air in the “mixing chamber” and is exhausted together as total flow. For each channel, the cavity pressure is measured
using a piezo-resistive manometer (IQP-500C, Bronkhorst GmbH). Operating at these “normal” conditions, the total residence
times within the instrument (filter changer exit until exhausted) are 0.43 s for the NO₃ channel and 0.34 s for the heated cavity.

130 **2.3 Mirror Mounting System**

The mirror mounting system is illustrated in Figure 2. Each cavity mirror is installed in a custom-made titanium mirror mount
and secured with a silicone O-ring plus retaining ring. The tilt adjustment of each mirror is achieved by three fine adjustment
screws (M4AS series, Thorlabs) that apply pressure at the locations highlighted with red dots in Figure 2a. This design offers
an optimal balance between easy adjustment and very stable positioning, which is critical for long-term cavity stability during
135 field campaigns. Figure 2b shows the mirror mount after its installation according to the schematic in Figure 1. The mirror
(red border) is secured in a separate chamber, which is continuously purged with clean air that enters the mixing chamber
(indigo border) after traversing a 42 mm long, 4 mm inner-diameter metal tube. The diameter of the tube is sufficient to guide
the laser beam through, but small enough to generate a high flow velocity that prevents back diffusion. After mixing, the
sample + clean air is exhausted as previously described. In this system, even the planar side of the mirrors is within the purged
140 volume as a window (WG10530-A, Thorlabs) prevents direct contact with ambient air and reduces the impact of changes in
ambient pressure on mirror alignment. All metallic components are sealed to the outside using silicone O-rings.

Figure 2c shows a photo of the combined mirror mount assembly within the instrument. In the centre, the laser enters through
the aforementioned window, while the adjacent fine adjustment screws set the mirror alignment and four wing screws are used
to easily disconnect the mirror mount for cleaning. When reinstalling, only very minor adjustments are required to optimize
145 the ring-down signal. At the top, the laser mount and 4 out of 8 of its fine-adjustment screws are shown. While the upper
screws are used to adjust the position of the collimation lens relative to the laser diode, the lower ones are used to adjust the
position of the laser mount for slight off-axis alignment to reduce back reflections into the laser diode, which can perturb the
laser emission spectrum.

In order to decrease thermal expansion related effects, each cavity uses three carbon-fibre reinforced polymer (CFRP) tubes
150 (1 m in length, 20 mm outer diameter, 1 mm wall thickness) mounted on custom-made, triangle-shaped, aluminium adapter
plates to stabilise the relative positions of the mirrors. This system is almost unaffected by vibrations or shocks and even after
strong impacts during container shipment only minor adjustments were required for optimal alignment.

2.4 Laser Optics and Emission Spectra

Two laser diodes (HL6545MG mounted in LDM21, Thorlabs) equipped with collimators (C610TME-A, Thorlabs) and optical
155 isolators (IO-3D-660-VLP, Thorlabs) provide light at ~ 662 nm for the cavities. Even with optical isolators in place, back-
reflection from the first cavity mirror into the laser diode resulted in random changes in transmitted laser intensity and/or



variations to the emission spectrum. Both caused additional noise to the ring-downs and therefore we avoid perfect on-axis alignment with this instrument. The central emission wavelength is matched to the peak absorption cross-section ($\lambda_{\max} \approx 662$ nm) of NO_3 by heating the laser diodes to 38-40 °C (TTC001 temperature controller, Thorlabs), as shown in Figure 3. The laser current is driven by a control board (MLDEVAL with MLD203CHB driver, Thorlabs), is externally modulated (see
160 Section 2.5) and results in an average optical power output of 8 mW (at 25 % duty cycle) after the optical isolator.

The laser diode emission is recorded using a compact spectrometer (630-684 nm, HR4000, OceanOptics). Its spectral resolution (~ 0.06 nm) was determined by calculating the full width at half maximum (FWHM) of seven spectral lines of neon from a low-pressure “Pen-Ray” lamp. We use an optical Y-fibre (BFY50HS02, Thorlabs) in front of the optical isolators to
165 collect a fraction of the light intensity at the edge of the laser. This enables us to monitor the output of both diodes simultaneously while individual emission spectra can be acquired by turning off the other laser. During normal operation, this process takes less than 2 seconds and is automated using a programmable USB-hub (EX-1596HMVS, EXSYS) which supplies power to the laser current drivers. By regularly recording the laser diode spectra (usually once per hour during field deployment), we can account for changes in the overlap of the laser emission and the NO_3 absorption cross-section, discussed
170 in Section 3.2.

At the other end of the cavity, transmitted light is detected by a photomultiplier tube (H10492-012, Hamamatsu) screened by an optical bandpass filter (10 nm FWHM @ 660 nm, 86-089, Edmund Optics) and located in a custom-designed housing to minimize stray light.

2.5 Signal Processing and Data Acquisition

175 For data acquisition, signal generation and initial visualization, we use a PXIe-1082 embedded computer including a PXIe-8840 Quad-Core processing unit manufactured by National Instruments (NI). The instrument’s system control has been programmed in LabVIEW and is based on the “Modular Multiple-Loop Application Framework” described in “The LabVIEW Style Book” (Blume, 2007).

In the same computer chassis, a PXIe-5413 function card is used to generate the modulation signal for the laser current drivers.
180 We use a square-wave function (625 Hz, 25 % duty cycle) at a sample rate of 2 MS/s. Data acquisition is performed by a PXI-6132 card (with a TB-2709 adapter for SMB connectors) running at the same sampling rate and is triggered by the rising edge of the modulation signal. Additionally, we use an external oscilloscope (TBS1104, Tektronix) to visualize the signals during alignment and operation.

For each recorded ring-down, we reject the initial 5 μs after switching off the laser and use the following 600 μs for fitting.
185 We pre-average 125 individual ring-downs to smoothen the signal and reduce computational load. Subsequently, we use the “linear regression of the sum” (LRS, Everest and Atkinson (2008)) algorithm to calculate the ring-down constant as used for similar instruments (Sobanski et al., 2016; Wagner et al., 2011). Afterwards, we use the average of five τ measurements to report 1 s data. We did not see a significant difference in the sensitivity of the instrument for different batch sizes of pre-averages.



190 3 Correction factors and overall uncertainty / precision

The uncertainty of NO_3 and N_2O_5 measurements is associated with a number of parameters and applied correction factors, including the effective absorption cross-section (σ), the ratio between the mirror distance and the actual absorption path length (R_L) and transmission factors which consider the loss of NO_3 in different parts of the instrument, such as the particle filters or cavity walls. While σ and R_L can be determined without measuring NO_3 , the transmission factors require the generation of NO_3 and N_2O_5 . In this section, we describe our preferred method of generating NO_3 , present our results of the instruments characterisation including its limit of detection, as well as provide new insights into the NO_3 transmission of PTFE filters. Concluding, we summarize all factors that contribute to the total measurement uncertainty.

3.1 Generation of NO_3 and N_2O_5

For most measurements we generated NO_3 and (mainly) N_2O_5 via the oxidation of NO with O_3 (R1, R2, R5) in a cylindrical, FEP-coated glass vessel (approx. 3 L volume, 60 cm length). 30-100 sccm of NO (1 ppmv) and 300-400 sccm of clean air (purified with CAP series, different manufacturers) with >15 ppmv of O_3 flowed into one end of the reactor where the mixture resided for more than 6 minutes in which time all NO was converted to either NO_2 , NO_3 or N_2O_5 . O_3 was generated by passing the clean air flow over a partially masked, 2-inch low-pressure mercury “Pen-Ray” lamp (10 mA, 78-2046-2, Jelight). After exiting the reactor, the N_2O_5 could optionally be thermally dissociated into NO_3 (and NO_2) by passage through a heated PFA segment (35 cm, 130 °C) directly before being diluted by about 17 standard litres per minute (slm) of clean air. The 17 slm were then sampled by both the 2CH-CRDS instrument and an ozone monitor (Model 205, 2B Technologies). We also used a 1 m³ environmental chamber into which N_2O_5 was flowed by passing clean air over N_2O_5 crystals held at about 200 K. This way both N_2O_5 and NO_3 in equilibrium were generated along with NO_2 . Alternatively, to generate NO_3 in the absence of N_2O_5 , the photolysis of ceric ammonium nitrate was used (Lambe et al., 2023). The chamber sources were found to have disadvantages including less stable mixing ratios over long time periods (when using N_2O_5 crystals) and the formation of high levels of water and HNO_3 when using the ceric ammonium nitrate source.

3.2 Determination of σ and R_L

To derive NO_3 mixing ratios according to Equation (1), we need measurements of σ and R_L . The effective absorption cross-section σ is calculated by the convolution of the emission spectra for each laser diode and the absorption spectrum of NO_3 . We use the temperature-dependent cross-sections reported by Orphal et al. (2003) and rescale the value at λ_{max} to the IUPAC recommendation (Iupac, 2025), which is $2.25 \times 10^{-17} \text{ cm}^2 \text{ molecule}^{-1}$ at 298 K, see Figure 3. The convoluted effective absorption cross-sections strongly depend on the gas temperature, with values of $\sigma(25 \text{ °C}) = 2.15 \times 10^{-17} \text{ cm}^2 \text{ molecule}^{-1}$ and $\sigma(100 \text{ °C}) = 1.55 \times 10^{-17} \text{ cm}^2 \text{ molecule}^{-1}$. As the laser diodes are temperature-stabilised, the effective cross-sections generally change by less than 5% over a period of several weeks. We estimate the uncertainty in the effective cross-sections to be 5% and 8% for the NO_3 and ($\text{NO}_3 + \text{N}_2\text{O}_5$) channel, respectively.



In order to determine R_L , we conducted experiments using ozone which absorbs at 662 nm albeit with a cross-section that is a factor ~ 10000 smaller than that of NO_3 at 298 K and 1 atm so that 10 ppbv (parts per billion by volume) of ozone is detected as ~ 1 pptv NO_3 -equivalent. For this experiment, about 7.3 ppmv of O_3 was produced by flowing 17 slm of clean air over a 7-inch mercury “Pen-Ray” lamp (10 mA, 78-2046-7, Jelight) and directed to the instrument. R_L was then determined by comparing the signal when O_3 was 1) present in both the purge gas flow and the cavity flow (i.e. absorption took place over the total mirror distance) or 2) was present only in the cavity flow (i.e. absorption took place over the actual absorption path length). This way R_L was determined to be 1.11 ± 0.02 for the NO_3 channel and 1.13 ± 0.06 for the ($\text{NO}_3 + \text{N}_2\text{O}_5$) channel. Both values are very similar to the geometric ratio of approximately 1.12 (= 74 cm / 66 cm).

3.3 NO_3 titration and the impact of $\text{NO} + \text{O}_3$

Accurate determination of NO_3 mixing ratios requires the complete removal of NO_3 during zero measurements. The fractional removal of NO_3 depends on the rate coefficient for the reaction between NO and NO_3 ($k_3 = 2.6 \times 10^{-11} \text{ cm}^3 \text{ molecule}^{-1} \text{ s}^{-1}$ at 298 K (Iupac, 2025)), the amount of added NO and the reaction time. With typical NO concentrations of about 100 ppbv, more than 99.996 % of the NO_3 is removed within the ~ 0.16 s reaction time available before the flow enters the cavity associated with the unheated channel. For the heated inlet of the ($\text{NO}_3 + \text{N}_2\text{O}_5$) channel, the NO_3 formed by thermal dissociation of N_2O_5 has less time to react with NO , which partially results from the time taken for N_2O_5 to dissociate and partially from the larger linear velocity in this part of the tubing. In order to fully dissociate the N_2O_5 we found that a temperature of 170 °C was required. Setting the temperature in the thermal dissociation inlet to this level also resulted in a homogeneous temperature along the absorption path within the cavity (which was kept at 100 °C). At these NO concentrations and temperatures, we need to correct our $\text{NO}_3 + \text{N}_2\text{O}_5$ measurements by a factor of 1.01 ± 0.01 in the heated channel. The discrepancy from unity stems from newly dissociated NO_3 , which requires additional time for complete titration. While this small correction introduces a minor systematic uncertainty, it reduces the impact of cavity wall losses, which would increase for lower flow rates, see Section 3.6.

This discrepancy could be decreased by increasing the amount of NO added, but this would subsequently increase the production of NO_2 via ambient O_3 (R1) and affects NO_3 measurements, since NO_2 and O_3 absorb (albeit weakly) at 662 nm. With a 662 nm cross-section of $\sim 4 \times 10^{-21} \text{ cm}^2 \text{ molecule}^{-1}$ for NO_2 at 294 K (Vandaele et al., 2002), its absorption cross-section is about twice that of O_3 at the same wavelength ($\sim 2 \times 10^{-21} \text{ cm}^2 \text{ molecule}^{-1}$ for O_3 at 293 K (Voigt et al., 2001)). Using the rate coefficient for the reaction of NO with O_3 of $k_1(298 \text{ K}) = 1.9 \times 10^{-14} \text{ cm}^3 \text{ molecule}^{-1} \text{ s}^{-1}$ (Iupac, 2025) and taking an O_3 level of 100 ppbv we calculate that about 2 ppbv of the O_3 would have been converted into NO_2 . Given the relative 662 nm cross sections of NO_3 , O_3 and NO_2 , this means that the loss of O_3 results in a negative offset of about -0.2 pptv NO_3 -equivalent, whereas the NO_2 formed results in a positive offset of +0.4 pptv NO_3 -equivalent. This results in an overestimation of the zero signal by up to +0.2 pptv for which corrections must be applied to the [NO_3] measurements.



In the heated ($\text{NO}_3 + \text{N}_2\text{O}_5$) channel, the rate coefficient for the reaction between NO and O_3 increases (by a factor of about three) to $k_1(373 \text{ K}) = 5.6 \times 10^{-14} \text{ cm}^3 \text{ molecule}^{-1} \text{ s}^{-1}$. Accounting for the shorter residence time and lower air density, about 3.5 ppbv of NO_2 are formed which corresponds to an overestimation of up to 0.35 pptv when assuming temperature-independent absorption cross-sections for NO_2 and O_3 at 662 nm.

Concluding, the major advantages of adding NO during zero measurements are rapid switching times, targeted removal of NO_3 and the negligible dilution of the sampled air (7 in 14000 = 0.05 %). Compared to other methods that sample/use clean air, we prevent changes in ambient concentration and therefore the absorption of other molecules like O_3 , NO_2 and water vapour remains constant. Especially, a correction of $[\text{H}_2\text{O}]$ would introduce a high uncertainty since its absorption spectrum exhibits sharp features at 662 nm (Schuster et al., 2009; Coheur et al., 2002) and its concentration can vary rather quickly during field measurements and greatly between ambient and clear air measurements.

3.4 Limit of Detection – Allan Deviation

Like most CRDS instruments, the major factor influencing the limit of detection (LOD) is the random variation (white noise) of the ring-down time, which depends on the adjustment of the cavity mirrors and changes of ambient conditions like pressure and temperature. The ideal LOD of the two channels was determined using Allan Deviation plots, where the 1σ (standard deviation) of the zero-signal is plotted against the integration time. The standard deviation decreases in the beginning due to averaging out of white noise and drift effects become more important for longer integration times. This results in a minimum, which can be interpreted as the best integration time for our instrument and is understood as the best achievable LOD of each channel.

Based on 1-second data, Figure 4 shows the Overlapping Allan Deviation (oadev by AllanTools.py version 2024.4) of our instrument under ideal laboratory conditions (stable temperatures, sampling particle-free clean air). The NO_3 channel (blue) has a LOD of less than 1 pptv at 1-second integration time. For the ($\text{NO}_3 + \text{N}_2\text{O}_5$) channel, this increases to about 2 pptv (1 s). The lowest deviation is achieved at integration times of about 3 and 12 minutes, when the LOD of the NO_3 channel is ~ 0.1 pptv and that of the ($\text{NO}_3 + \text{N}_2\text{O}_5$) channel < 0.2 pptv, respectively. Based on this, we determined the ideal time between zero measurements to be 3 minutes to minimize the influence of drifts while still being frequent enough to capture atmospheric variability.

During field measurements, we determine the LOD (for a certain period of time) as the maximum of either 2σ of all zero data points (“white noise”) or 2σ of all absolute differences between consecutive zero measurements (“drift”). This holds for 1-second resolution, but is divided by the \sqrt{n} when resampling to a different resolution if the white noise is dominating. Here, n denotes the number of zero data point that are within the resampling interval on average (e.g., $n = 8/3$ when resampling to 1-minute resolution since 8 zero data points are recorded every 3 minutes). Typical values range from 1-2 pptv for the NO_3 channel and 3-5 pptv for the ($\text{NO}_3 + \text{N}_2\text{O}_5$) channel and are dominated by white noise from zero measurements.



3.5 NO₃ transmission of PTFE filters

As previously mentioned, CRDS-based measurements of ambient NO₃ are usually operated with inlet filters to prevent spurious signals due to particle scattering and to hinder contamination of the cavity mirrors. Several CRDS instruments that measure NO₃ have used R2PJ047 PTFE membrane filters by Pall Corporation (2 μm pore size, 25 μm thickness and 47 mm in diameter). These filters have been shown to have good transmission for NO₃ and previous studies have reported clean filter transmission factors in the ranges of 86 ± 5 % (Brown et al., 2002), 90 ± 3 % (Crowley et al., 2010) and 93 ± 2 % (Dubé et al., 2006). As these filters are no longer produced, we have explored alternative products from Merck Millipore (PM2547050, 40 μm thickness) and Cytiva Whatman (7592-104, 40 μm thickness), where the PTFE membrane is supported by a polypropylene ring of similar width. Operating at normal conditions and a sample flow of 14 slm, Pall filters cause a pressure drop of about 10 mbar compared to an empty filter holder; those from Merck and Cytiva show a pressure drop of approximately 20 mbar.

We measured the transmission of NO₃ for different batches of unused filters using the NO+O₃ flow tube source which produced about 500 ppbv of O₃ and more than 100 pptv of NO₃ after the dilution. The fractional transmission of NO₃ was determined by measuring its mixing ratio after passage through an empty custom-made filter holder (FEP-coated aluminium, wire bail lid system with silicone O-ring seal) or through the same filter holder equipped with a filter. This type of filter holder has a more reliable closing mechanism than commercial PFA inline filter holders with a screw lock. Figure 5 shows the time dependent NO₃ transmission through the Pall and Merck filters. The initial NO₃ transmission of the filters is variable and ranges from 0.7 to 0.9, which is similar to measurements shown by Brown et al. (2002) where the initial transmission ranged from 0.6 to 0.8. Continuous exposure to NO₃ and O₃ increases the filter transmission to its maximum within 5 to 10 minutes. The same behaviour was observed during the comparison between Pall and Cytiva filters, see Figure S1 in the Supplement. We approximate this exponentially increasing behaviour by Equation (3) to determine the asymptotic maximum transmission factor T_{max} .

$$T(t) = T_{max} - A * \exp(-kt) \quad (3)$$

where t is the exposure time, k is a coefficient that defines the time-constant for “cleaning” the filter and A is used to adjust the amplitude of the exponential contribution. An overview of the comparison of unused filters is presented in Table 1 and shows that all tested filters achieve a maximum NO₃ transmission of about 98 ± 4 % which is the mean and two standard deviations of all determined T_{max} values. Additional details of the procedure and results for different filters are presented in Section S1. Our experiments indicate that initially reactive PTFE filters can be made passive for NO₃ by sufficient exposure to NO₃ and O₃. As the loss of NO₃ to filters can be associated with the presence of unsaturated hydrocarbons adsorbed to the filter (Tang et al., 2010), we explored the potential to re-use filters that had become reactive towards NO₃ during exposure to ambient air. As O₃ is known to react with olefins (Cox et al., 2020), we determined the NO₃ transmission of filters that had been exposed to high concentrations of O₃ (100 sccm of more than 5 % O₃ in O₂) for a few minutes. For these experiments, O₃ was generated using a commercial, electrical discharge ozone generator (COM-CD-HF4, Anseros) supplied with oxygen 5.0



at 1 bar. Using this method, we were able to fully restore the 98 ± 4 % transmission of previously aged and reactive filters, see Figure S2.

Our results indicate that fresh filters are more reactive to NO_3 than those that have been treated with O_3 . Therefore, during operation in the field, the stack of filters (held in the automatic filter changer) is flushed continuously by 500 sccm of dry, clean air containing about 15 ppmv of O_3 prior to use. Using this setup the NO_3 transmission for fresh (or freshly passivated) filters from Pall and Merck is 98 ± 4 % while for untreated PTFE filters a value of 90 ± 5 % is appropriate and consistent with that reported by Brown et al. (2002) and Crowley et al. (2010). Filters by Cytiva were not tested during field measurements, only in the laboratory.

Note that while such procedures can optimize the initial transmission of the filters for NO_3 , contamination and loss of transmission during sampling of ambient air will occur at different rates depending on, e.g. particle concentrations and composition. Under polluted conditions, this may imply that filter changes every 30 minutes are necessary, whereas every 2 hours may be adequate for more remote locations. When using the automatic filter changer, an additional NO_3 transmission factor must be considered and was determined by comparing measured $[\text{NO}_3]$ between the path through the filter changer and a PFA bypass with negligible NO_3 loss (Schuster et al., 2009). Switching between the two paths multiple times yielded an average transmission of 80 ± 5 % caused by wall losses along the sample path.

3.6 Losses of NO_3 on the cavity walls

The fractional loss of NO_3 to the cavity walls can be a major correction factor for CRDS instruments and depends on the residence time in the cavity and on the material from which the cavity is made. Common materials are PFA tubing (Wagner et al., 2011; Fuchs et al., 2008) or cavities made from glass or metal that are either coated with a halocarbon wax (Dubé et al., 2006; Brown et al., 2002) or FEP (Sobanski et al., 2016; Schuster et al., 2009).

In order to reduce NO_3 losses, our glass cavities are coated with FEP and operated at short residence times (i.e. high flow rates), as described in Section 2.2. As the loss of NO_3 is a first-order process, we quantify the wall loss rate constant (k_w) by varying the residence time in each channel and observing the relative change in the NO_3 signal. To avoid changes in either the NO_3 concentration or its loss in inlet lines, the total flow (i.e. to both cavities) is kept constant during these experiments and the filter is bypassed. Figure 6 shows the expected exponential decrease in NO_3 with increasing residence time. The residence times were calculated from the flow rates and are shorter in the heated inlet / cavity due to the increase in linear velocity at high temperatures. In the heated channel, measurements below flow rates of 5000 sccm were excluded due to increased noise in the ring-down signal, caused by increased heat uptake that affected the optical alignment. This is reproducible and a similar effect was already observed by Sobanski et al. (2016).

Each data point in Figure 6 represents an average of 3 minutes. The values of k_w obtained are $0.15 \pm 0.06 \text{ s}^{-1}$ for the NO_3 channel and $0.45 \pm 0.20 \text{ s}^{-1}$ for the ($\text{NO}_3 + \text{N}_2\text{O}_5$) channel. The more rapid loss of NO_3 in the hot cavity may be related to increased collision rates of NO_3 with the surface. Under normal operating conditions (7 slm each channel), the residence times are 0.43 s in the NO_3 cavity and 0.34 s in the ($\text{NO}_3 + \text{N}_2\text{O}_5$) cavity, which translate to wall loss factors of 0.94 ± 0.03 and



0.86 ± 0.06, respectively. These values are very similar to other instruments that reported losses in the range of 5 % to 15 %
 350 (Dubé et al., 2006; Schuster et al., 2009; Sobanski et al., 2016; Brown et al., 2002).

3.7 Calculation of Ambient Mixing Ratios and Total Measurement Uncertainty

The true ambient NO₃ mixing ratios can be derived from Equation (4) which considers the transmission factors originating from the filter changer (T_{FC}), filters (T_{Filter}) and wall loss of NO₃ (T_{NO₃, unheated}) for the unheated cavity. The complete overview of all cavity specific values is presented in Table 2.

$$355 \quad [\text{NO}_3] = \frac{[\text{NO}_3]_{\text{measured}}}{T_{\text{FC}} \cdot T_{\text{Filter}} \cdot T_{\text{NO}_3, \text{unheated}}} \quad (4)$$

Note that [NO₃]_{measured} is determined by Equation (1). To derive the expression for true ambient [N₂O₅], we start with an expression for [NO₃ + N₂O₅]_{measured} which is corrected by a minor factor due to the short reaction time of newly dissociated NO₃ with NO (C_{dissoc}), see Section 3.3.

$$C_{\text{dissoc}} \cdot [\text{NO}_3 + \text{N}_2\text{O}_5]_{\text{measured}} = T_{\text{FC}} \cdot T_{\text{Filter}} \cdot T_{\text{NO}_3, \text{heated}} \cdot [\text{NO}_3] + T_{\text{N}_2\text{O}_5} \cdot T_{\text{NO}_3, \text{heated}}^* \cdot [\text{N}_2\text{O}_5] \quad (5)$$

360 Here, we applied the respective transmission factors to [NO₃] and [N₂O₅]. Please note that there is a different NO₃ transmission factor for the heated cavity (T_{NO₃, heated}) and slightly higher transmission (T_{NO₃, heated}^{*}) for newly formed NO₃ after the dissociation of N₂O₅, which was derived by the corresponding wall loss rate and the residence time purely within the absorption path of the cavity (about 0.24 s). The loss of N₂O₅ in transmission through filters and inert PFA tubing (T_{N₂O₅}) has been shown to be negligible (Schuster et al., 2009; Brown et al., 2002) but is listed for completeness. By rearranging Equation (5) and
 365 inserting Equation (4), we derive an expression for the true ambient N₂O₅ which depends on the measurements of both cavities and is similar to the one shown by Fuchs et al. (2008):

$$[\text{N}_2\text{O}_5] = \frac{C_{\text{dissoc}} \cdot [\text{NO}_3 + \text{N}_2\text{O}_5]_{\text{measured}} - \frac{T_{\text{NO}_3, \text{heated}}}{T_{\text{NO}_3, \text{unheated}}} \cdot [\text{NO}_3]_{\text{measured}}}{T_{\text{N}_2\text{O}_5} \cdot T_{\text{NO}_3, \text{heated}}^*} \quad (6)$$

The total measurement uncertainty (TMU) includes contributions from the absorption cross-section of NO₃, the ratio between
 370 mirror distance and absorption path length as well as the aforementioned NO₃ transmission factors. The overview of all uncertainties is listed in Table 2. Based on this, we determine the TMU as propagated relative uncertainty and estimate 9.8 % for the measurements of [NO₃] in the unheated cavity. Due to the subtraction within Equation (6), this method becomes slightly more complicated for N₂O₅ and can be most easily derived by redefining the individual terms:

- I. $x \equiv [\text{N}_2\text{O}_5]$
- 375 II. $a \equiv [\text{NO}_3 + \text{N}_2\text{O}_5]_{\text{measured}} \cdot C_{\text{dissoc}}$
- III. $b \equiv [\text{NO}_3]_{\text{measured}} \cdot \frac{T_{\text{NO}_3, \text{heated}}}{T_{\text{NO}_3, \text{unheated}}}$
- IV. $c \equiv T_{\text{N}_2\text{O}_5} \cdot T_{\text{NO}_3, \text{heated}}^*$
- V. $y \equiv x \cdot c = a - b$

380 We derive the relative uncertainty (written in parenthesis) of $y = a - b$ by:



$$\left(\frac{\Delta y}{y}\right) = \frac{\sqrt{\Delta a^2 + \Delta b^2}}{|a-b|} = \frac{\sqrt{a^2 \cdot \left(\frac{\Delta a}{a}\right)^2 + b^2 \cdot \left(\frac{\Delta b}{b}\right)^2}}{|a| \cdot \left|1 - \frac{b}{a}\right|} = \frac{\sqrt{\left(\frac{\Delta a}{a}\right)^2 + \frac{b^2}{a^2} \left(\frac{\Delta b}{b}\right)^2}}{\left|1 - \frac{b}{a}\right|} = \frac{\sqrt{\left(\frac{\Delta a}{a}\right)^2 + r^2 \cdot \left(\frac{\Delta b}{b}\right)^2}}{|1-r|} \quad (7)$$

In the last step, we defined $r = \frac{b}{a}$ (with $a > 0$) which represents the ratio between (b) the proportion of NO_3 detected in the heated cavity over (a) the corrected sum of $\text{NO}_3 + \text{N}_2\text{O}_5$. Furthermore, we derive the relative uncertainty of $[\text{N}_2\text{O}_5] = x = y / c$ which can be written as:

$$\left(\frac{\Delta x}{x}\right) = \sqrt{\left(\frac{\Delta y}{y}\right)^2 + \left(\frac{\Delta c}{c}\right)^2} = \sqrt{\frac{\left(\frac{\Delta a}{a}\right)^2 + r^2 \cdot \left(\frac{\Delta b}{b}\right)^2}{|1-r|^2} + \left(\frac{\Delta c}{c}\right)^2} \quad (8)$$

This depends only on the relative uncertainties of a , b and c which depend on the presented (and propagated) uncertainties of this instrument as well as r . A more intuitive understanding of r can be gained by its relation to ambient $[\text{NO}_2]$ and the equilibrium constant (K_{eq}) that together with the NO_2 concentration and the temperature defines the $\text{NO}_3 / \text{N}_2\text{O}_5$ ratio (Iupac, 2025; Burkholder et al., 2020; Osthoff et al., 2007). Since r is defined by NO_3 and N_2O_5 measured (and corrected) in the heated cavity, we can rewrite:

$$r = \frac{[\text{NO}_3]_{\text{heated}}}{[\text{NO}_3]_{\text{heated}} + [\text{N}_2\text{O}_5]_{\text{heated}}} = \frac{[\text{NO}_3] \cdot d}{[\text{NO}_3] \cdot d + [\text{N}_2\text{O}_5] \cdot c} = \left(1 + \frac{[\text{N}_2\text{O}_5]}{[\text{NO}_3]} \cdot \frac{c}{d}\right)^{-1} = \left(1 + K_{eq} \cdot [\text{NO}_2] \cdot \frac{c}{d}\right)^{-1} \quad (9)$$

With c and $d = T_{\text{FC}} \cdot T_{\text{Filter}} \cdot T_{\text{NO}_3, \text{heated}}$ describing the combined transmission factors of the respective molecules within the heated channel. Concluding, we can estimate the TMU of the heated channel based on an additional ambient $[\text{NO}_2]$ measurement and well-known constants for the thermal equilibrium as well as the transmission factors of this instrument.

The lowest uncertainty of $x = [\text{N}_2\text{O}_5]$ is reported when $r \rightarrow 0$ (e.g. ambient temperature $< 0^\circ\text{C}$ and $[\text{NO}_2] > 2$ ppbv results in $r < 3\%$) and yields 11.5 % while we estimate about 22.3 % for $r = 0.5$ (i.e. $[\text{NO}_3] = [\text{N}_2\text{O}_5]$). A graphic of this estimate is shown in Figure S3 and highlights the case for $r \rightarrow 1$ (i.e. very low $[\text{N}_2\text{O}_5]$) when the subtraction introduces uncertainties greater than 100 %. Please note that the (atmospheric) variability of $[\text{NO}_3]_{\text{measured}}$ and $[\text{NO}_3 + \text{N}_2\text{O}_5]_{\text{measured}}$ does not contribute to the TMU estimation but uncertainties of σ and R_L for both cavities are included.

Another potential uncertainty is the thermal dissociation of N_2O_5 to NO_3 during transit through the filter changer and cavities, and becomes important when sampling cold air into a warm container / instrument (Schuster et al., 2009). Assuming an equilibrium of NO_3 and N_2O_5 at 1 ppbv of NO_2 and no additional loss or production, an immediate increase from 0°C to 25°C causes the dissociation of about 1 % of N_2O_5 in 0.25 seconds, which is the residence time from the filter changer entrance to the cavity entrance. This increases to about 2 % until the exit of the cavity (after 0.55 seconds) and has to be corrected when there is a significant temperature difference compared to ambient conditions.



4 Field measurements

410 The performance of this 2CH-CRDS instrument under field conditions is illustrated by data from a recent field campaign, which took place in May 2025 at the Taunus Observatory at the summit of Kleiner Feldberg (825 m above sea level), Germany. The instrument was located in a modified sea container and sampled from a high-volume flow inlet (about 30 cm in diameter, centerline velocity of 20 m s^{-1}) from 5 m above ground. In combination with an additional bypass flow ($\sim 25000 \text{ sccm}$ through 2 m of 1/2-inch PFA tubing) the residence time within the container inlet is estimated to be about 0.4 s.

415 At the same inlet, a commercial ozone monitor (Model 205, 2B Technologies, LOD 2 ppb, uncertainty 5 %) monitored the mixing ratios of O_3 and a chemiluminescence detection (CLD) instrument measured NO and NO_2 (LOD 4 pptv for NO and 5 pptv for NO_2 , total uncertainty 5 %) (Nussbaumer et al., 2021). Ambient temperature was recorded by a small weather station (DNT000008, dnt) which was mounted at the same height as the inlet about 2.5 m horizontally distant, and compared to the measurements of the German Meteorological Service (DWD, station ID 2601) located about 15 m to the east and only 2 m
420 above the ground.

In Figure 7, we present our measurements from 13–14 May, which was at the beginning of the campaign during a dry and stable period (see Figure S4 for meteorological data). During this night, the ambient temperature decreased from 12 to $10 \text{ }^\circ\text{C}$ while relative humidity was about 50 to 55 %. Wind speeds decreased from 5 to 2 m s^{-1} and gradually changed from North-East to South-East. O_3 was consistently between 61 and 65 ppbv with a brief increase shortly before 01:00 UTC. Due to a
425 calibration, NO and NO_2 measurements only started at 21:00 UTC. Until sunrise at $\sim 03:30 \text{ UTC}$ (vertical black line), [NO] remained below LOD since its lifetime is less than 1 minute at $[\text{O}_3] > 60 \text{ ppbv}$ and ambient temperatures above $10 \text{ }^\circ\text{C}$. NO was observed after dawn when its production via the photolysis of NO_3 and NO_2 occurred. $[\text{NO}_2]$ decreased from 750 to 500 pptv at the end of the night. Again, at about 1 UTC, an increase by $\sim 100 \text{ pptv}$ for approx. 20 minutes was observed as well as smaller fluctuations thereafter, indicating changes in air mass composition.

430 This night, the 2CH-CRDS operated at a LOD of 1 pptv for NO_3 and 3 pptv for the $\text{NO}_3+\text{N}_2\text{O}_5$ cavity at 1-minute integration time, which is determined by the variability of zero measurements and drift effects. Both NO_3 and N_2O_5 increased quasi-continuously from sunset until dawn, with NO_3 mixing ratios reaching 20 pptv shortly before sunrise, before rapidly decreasing due to photolysis. The maximum N_2O_5 mixing ratio ($\sim 40 \text{ pptv}$) was also observed at the end of the night. Maxima in the N_2O_5 mixing ratio were correlated with NO_2 mixing ratios, indicating that the variability was driven (at least partially) by an increase
435 in the NO_3 production term. In Figure 7e, we show temperature-dependent equilibrium constants based on the JPL (Jet Propulsion Laboratory) recommended values and associated uncertainties (Burkholder et al., 2020) alongside the calculated values based on our measurements using $K_{\text{eq}} = [\text{N}_2\text{O}_5] / ([\text{NO}_3] \times [\text{NO}_2])$. We calculated the upper and lower limits by considering the LODs for each measurement and their uncertainties presented earlier.

Based on Crowley et al. (2010), the time to relax to equilibrium ($\tau_{\text{eq}} = (k_5 \times [\text{NO}_2] + k_6)^{-1}$ with corresponding reaction rates
440 (Iupac, 2025)) was about 150 seconds over the course of this night, which is sufficiently short to expect NO_3 and N_2O_5 to remain in thermal equilibrium. During the latter hours of the night (after 01:00 UTC), the measured K_{eq} is in good agreement



with the recommended value. Before 23:00 UTC, when $[\text{NO}_3]$ remained mostly below 5 pptv, our calculated values of K_{eq} are higher (by a factor of about 1.4) than expected but still agree within the combined uncertainty.

445 The discrepancy in K_{eq} before 23:00 UTC could also be associated with uncertainty in the ambient temperature used in the calculation. This could result from measurement uncertainty (e.g. insufficiently precise calibration of the temperature sensor) or from the air mass having recently experienced a different temperature (i.e. due to vertical gradients in temperature) than measured at the inlet. Changing the temperature by 1 °C would result in values of K_{eq} that would encompass most of the measured values. In addition, a very local sink of NO_3 or N_2O_5 or a loss of either on the inlet material (e.g. via accumulation of reactive aerosol) could also preclude calculation of the correct value of K_{eq} as previously reported (Crowley et al., 2011).

450 In summary, while several factors contribute to the non-perfect agreement in K_{eq} derived either from our measurements of NO_2 , NO_3 , N_2O_5 and temperature or from the recommended, temperature-dependent parameterisation, both agree within the combined uncertainties.

5 Conclusion

We have developed and characterized a new 2CH-CRDS instrument to quantify the mixing ratio of NO_3 and N_2O_5 of ambient
455 air. The instrument's compact size and relatively low weight allow for measurements at remote locations where transport and installation space are limited. Under laboratory conditions, we achieved LODs of about 0.1 pptv for the NO_3 channel and 0.2 pptv for the ($\text{NO}_3 + \text{N}_2\text{O}_5$) channel (1σ Allan deviation at 3-minute integration time). Under field conditions LODs are more typically 1 pptv and 3 pptv (2σ variations of zero measurements at 1-min resolution), respectively.

The instrument produced reliable field measurements of NO_3 and N_2O_5 , which (in combination with measurements of NO_2)
460 agree within their uncertainty with equilibrium calculations based on the recommended values. We estimated the total measurement uncertainty for $[\text{NO}_3]$ to be 9.8 % and presented an equation to determine the TMU for $[\text{N}_2\text{O}_5]$ depending on the ratio of ambient NO_3 and N_2O_5 , which can also be derived by the equilibrium constant and ambient $[\text{NO}_2]$. As a lower limit, we estimate 11.5 % ($[\text{NO}_2] > 2$ ppbv, $T < 0$ °C) which increases to about 22.3 % for $[\text{NO}_3] \approx [\text{N}_2\text{O}_5]$.

Extensive testing of filters from Merck Millipore (PM2547050) and Cytiva Whatman (7592-104) proved them to be viable
465 alternatives to the discontinued PTFE filters from Pall (R2PJ047). Both Merck and Cytiva filters (but also filters from Pall) showed an initial NO_3 transmission of about 80 %, which could be increased to > 98 % after 5-10 minutes of exposure to NO_3 and O_3 . Exposure of filters, while stacked in our automatic filter changer, to a stream of O_3 (500 sccm of about 20 ppmv) in clean air results in > 98 % transmission of NO_3 directly after each filter change. In addition, we showed that the transmission of NO_3 through used filters can be optimised by treatment with large concentrations of O_3 , thus enabling their reuse while
470 reducing waste and costs.



6 Data availability

Data underlying the figures in this publication will be made available on the Max Planck repository (EDMOND) after the acceptance of the manuscript.

7 Author contributions

- 475 Conceptualization: GT, JS, JC.
Data Curation: GT, SA, PD.
Formal Analysis: GT.
Funding Acquisition: JL, JC.
Investigation: GT, SA, PD, JS, JC.
- 480 Methodology: GT, JC.
Project Administration: JL, JC.
Resources: GT, JS, JL, JC.
Software: GT.
Supervision: JL, JC.
- 485 Validation: GT.
Visualization: GT.
Writing – original draft: GT, JC.
Writing – review & editing: GT, SA, PD, JS, JL, JC.

8 Competing interests

- 490 The contact authors have declared that none of the authors has any competing interests.

9 Acknowledgements

- SA thanks the Alexander von Humboldt foundation for funding her stay at the MPIC. We thank the following: Uwe Parchatka (MPIC) and Marcel Zauner-Wieczorek (Goethe University Frankfurt) for their support throughout the campaign at Kleiner Feldberg; Chemours for providing a sample of the FEED-121 solution used to coat the cavity glass walls; Merck Millipore and
- 495 Cytiva Whatman for providing each a sample of PTFE filters for our transmission measurements. This work was supported by the “Max Planck Graduate Center” (MPGC) with the Johannes Gutenberg University of Mainz.



References

- Aliwell, S. R. and Jones, R. L.: Measurements of tropospheric NO₃ at midlatitude, *J. Geophys. Res. -Atmos.*, 103, 5719-5727, 1998.
- Allan, B. J., Plane, J. M. C., Coe, H., and Shillito, J.: Observations of NO₃ concentration profiles in the troposphere, *J. Geophys. Res. -Atmos.*, 107, 4588, doi: 10.1029/2002jd002112, 2002.
- Atkinson, R. and Arey, J.: Atmospheric degradation of volatile organic compounds, *Chem. Rev.*, 103, 4605-4638, 10.1021/cr0206420, 2003.
- Ayers, J. D. and Simpson, W. R.: Measurements of N₂O₅ near Fairbanks, Alaska, *J. Geophys. Res. -Atmos.*, 111, 2006.
- Ayers, J. D., Apodaca, R. L., Simpson, W. R., and Baer, D. S.: Off-axis cavity ringdown spectroscopy: application to atmospheric nitrate radical detection, *Appl. Opt.*, 44, 7239-7242, 2005.
- Berden, G., Peeters, R., and Meijer, G.: Cavity ring-down spectroscopy: Experimental schemes and applications, *International Reviews in Physical Chemistry*, 19, 565-607, 2000.
- Blume, P. A.: *The LabVIEW Style Book*, Prentice Hall 2007.
- Brown, S. S. and Stutz, J.: Nighttime radical observations and chemistry, *Chem. Soc. Rev.*, 41, 6405-6447, 2012.
- Brown, S. S., Stark, H., Ciciora, S. J., and Ravishankara, A. R.: In-situ measurement of atmospheric NO₃ and N₂O₅ via cavity ring-down spectroscopy, *Geophys. Res. Lett.*, 28, 3227-3230, 2001.
- Brown, S. S., Stark, H., Ciciora, S. J., McLaughlin, R. J., and Ravishankara, A. R.: Simultaneous in situ detection of atmospheric NO₃ and N₂O₅ via cavity ring-down spectroscopy, *Rev. Sci. Instrum.*, 73, 3291-3301, 2002.
- Brown, S. S., Dube, W. P., Osthoff, H. D., Wolfe, D. E., Angevine, W. M., and Ravishankara, A. R.: High resolution vertical distributions of NO₃ and N₂O₅ through the nocturnal boundary layer, *Atmos. Chem. Phys.*, 7, 139-149, 2007.
- Brown, S. S., Stark, H., Ryerson, T. B., Williams, E. J., Nicks, D. K., Trainer, M., Fehsenfeld, F. C., and Ravishankara, A. R.: Nitrogen oxides in the nocturnal boundary layer: Simultaneous in situ measurements of NO₃, N₂O₅, NO₂, NO, and O₃, *J. Geophys. Res. -Atmos.*, 108, art. 4299, 10.1029/2002JD002917, 2003.
- Burkholder, J., Sander, S., Abbatt, J., Barker, J., Cappa, C., Crounse, J., Dibble, T., Huie, R., Kolb, C., and Kurylo, M.: Chemical kinetics and photochemical data for use in atmospheric studies; evaluation number 19, Jet Propulsion Laboratory, National Aeronautics and Space Administration, 2020.
- Carslaw, N., Plane, J. M. C., Coe, H., and Cuevas, E.: Observations of the nitrate radical in the free troposphere at Izana de Tenerife, *J. Geophys. Res. -Atmos.*, 102, 10613-10622, 1997.
- Coheur, P. F., Fally, S., Carleer, M., Clerbaux, C., Colin, R., Jenouvrier, A., Merienne, M. F., Hermans, C., and Vandaele, A. C.: New water vapor line parameters in the 26000-13000 cm⁻¹ region, *J. Quant. Spectrosc. Radiat. Transfer*, 74, 493-510, 10.1016/s0022-4073(01)00269-2, 2002.
- Cox, R. A., Ammann, M., Crowley, J. N., Herrmann, H., Jenkin, M. E., McNeill, V. F., Mellouki, A., Troe, J., and Wallington, T. J.: Evaluated kinetic and photochemical data for atmospheric chemistry: Volume VII – Criegee intermediates, *Atmos. Chem. Phys.*, 20, 13497-13519, 10.5194/acp-20-13497-2020, 2020.
- Crowley, J. N., Schuster, G., Pouvesle, N., Parchatka, U., Fischer, H., Bonn, B., Bingemer, H., and Lelieveld, J.: Nocturnal nitrogen oxides at a rural mountain site in south-western Germany, *Atmos. Chem. Phys.*, 10, 2795-2812, 2010.
- Crowley, J. N., Thieser, J., Tang, M. J., Schuster, G., Bozem, H., Hasaynali Beygi, Z., Fischer, H., Diesch, J.-M., Drewnick, F., Borrmann, S., Song, W., Yassaa, N., Williams, J., Pöhler, D., Platt, U., and Lelieveld, J.: Variable lifetimes and loss mechanisms for NO₃ and N₂O₅ during the DOMINO campaign: Contrast between marine, urban and continental air, *Atmos. Chem. Phys.*, 11, 10863-10870, 2011.
- Dorn, H. P., Apodaca, R. L., Ball, S. M., Brauers, T., Brown, S. S., Crowley, J. N., Dubé, W. P., Fuchs, H., Häseler, R., Heitmann, U., Jones, R. L., Kiendler-Scharr, A., Labazan, I., Langridge, J. M., Meinen, J., Mentel, T. F., Platt, U., Pöhler, D., Rohrer, F., Ruth, A. A., Schlosser, E., Schuster, G., Shillings, A. J. L., Simpson, W. R., Thieser, J., Tillmann, R., Varma, R., Venables, D. S., and Wahner, A.: Intercomparison of NO₃ radical detection instruments in the atmosphere simulation chamber SAPHIR, *Atmos. Meas. Tech.*, 6, 1111-1140, 10.5194/amt-6-1111-2013, 2013.
- Dubé, W. P., Brown, S. S., Osthoff, H. D., Nunley, M. R., Ciciora, S. J., Paris, M. W., McLaughlin, R. J., and Ravishankara, A. R.: Aircraft instrument for simultaneous, in situ measurement of NO₃ and N₂O₅ via pulsed cavity ring-down spectroscopy, *Rev. Sci. Instrum.*, 77, doi: 10.1063/1.2176058, 2006.



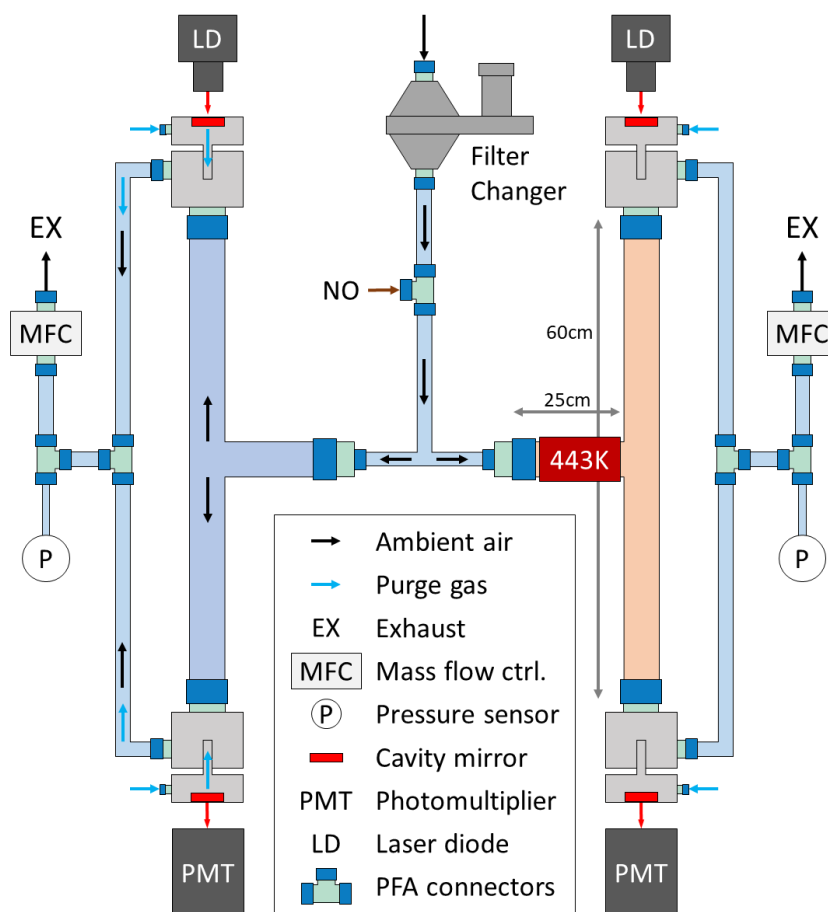
- Everest, M. A. and Atkinson, D. B.: Discrete sums for the rapid determination of exponential decay constants, *Rev. Sci. Instrum.*, 79, 10.1063/1.2839918, 2008.
- Finlayson-Pitts, B. J. and Pitts, J. N.: *Chemistry of the upper and lower atmosphere*, Academic Press, San Diego 2000.
- 550 Fuchs, H., Dube, W. P., Cicciola, S. J., and Brown, S. S.: Determination of inlet transmission and conversion efficiencies for in situ measurements of the nocturnal nitrogen oxides, NO₃, N₂O₅ and NO₂, via pulsed cavity ring-down spectroscopy, *Anal. Chem.*, 80, 6010-6017, 2008.
- Geyer, A., Ackermann, R., Dubois, R., Lohrmann, B., Muller, T., and Platt, U.: Long-term observation of nitrate radicals in the continental boundary layer near Berlin, *Atmos. Env.*, 35, 3619-3631, 10.1016/S1352-2310(00)00549-5, 2001.
- 555 Geyer, A., Alicke, B., Ackermann, R., Martinez, M., Harder, H., Brune, W., di Carlo, P., Williams, E., Jobson, T., Hall, S., Shetter, R., and Stutz, J.: Direct observations of daytime NO₃: Implications for urban boundary layer chemistry, *J. Geophys. Res. -Atmos.*, 108, 10.1029/2002JD002967 2003.
- IUPAC Task Group on Atmospheric Chemical Kinetic Data Evaluation, (Ammann, M., Cox, R.A., Crowley, J.N., Herrmann, H., Jenkin, M.E., McNeill, V.F., Mellouki, A., Rossi, M. J., Troe, J. and Wallington, T. J.). Last access Sept. 2025: <https://iupac.aeris-data.fr/>, last
- 560 Lambe, A. T., Bai, B., Takeuchi, M., Orwat, N., Zimmerman, P. M., Alton, M. W., Ng, N. L., Freedman, A., Clafin, M. S., Gentner, D. R., Worsnop, D. R., and Liu, P.: Technical note: Gas-phase nitrate radical generation via irradiation of aerated ceric ammonium nitrate mixtures, *Atmos. Chem. Phys.*, 23, 13869-13882, 10.5194/acp-23-13869-2023, 2023.
- Matsumoto, J., Imai, H., Kosugi, N., and Kaji, Y.: In situ measurement of N₂O₅ in the urban atmosphere by thermal decomposition/laser-induced fluorescence technique, *Atmos. Env.*, 39, 6802-6811, 2005.
- 565 Mazurenka, M., Orr-Ewing, A. J., Peeverall, R., and Ritchie, G. A. D.: Cavity ring-down and cavity enhanced spectroscopy using diode lasers, *Annu. Rep. Prog. Chem., Sect C*, 101, 100-142, 2005.
- Ng, N. L., Brown, S. S., Archibald, A. T., Atlas, E., Cohen, R. C., Crowley, J. N., Day, D. A., Donahue, N. M., Fry, J. L., Fuchs, H., Griffin, R. J., Guzman, M. I., Herrmann, H., Hodzic, A., Iinuma, Y., Jimenez, J. L., Kiendler-Scharr, A., Lee, B. H., Luecken, D. J., Mao, J., McLaren, R., Mutzel, A., Osthoff, H. D., Ouyang, B., Picquet-Varrault, B., Platt, U., Pye, H. O. T., Rudich, Y., Schwantes, R. H., Shiraiwa, M., Stutz, J., Thornton, J. A., Tilgner, A., Williams, B. J., and Zaveri, R. A.: Nitrate radicals and biogenic volatile organic compounds: oxidation, mechanisms, and organic aerosol, *Atmos. Chem. Phys.*, 17, 2103-2162, 10.5194/acp-17-2103-2017, 2017.
- Noxon, J. F., Norton, R. B., and Henderson, W. R.: Observation of Atmospheric NO₃, *Geophys. Res. Lett.*, 5, 675-678, 1978.
- 575 Nussbaumer, C. M., Parchatka, U., Tadic, I., Bohn, B., Marno, D., Martinez, M., Rohloff, R., Harder, H., Kluge, F., Pfeilsticker, K., Obersteiner, F., Zöger, M., Doerich, R., Crowley, J. N., Lelieveld, J., and Fischer, H.: Modification of a conventional photolytic converter for improving aircraft measurements of NO₂ via chemiluminescence, *Atmos. Meas. Tech.*, 14, 6759-6776, 10.5194/amt-14-6759-2021, 2021.
- Orphal, J., Fellows, C. E., and Flaud, P. M.: The visible absorption spectrum of NO₃ measured by high-resolution Fourier transform spectroscopy, *J. Geophys. Res. -Atmos.*, 108, Art. Nr. 4077, doi:10.1029/2002JD002489, 2003.
- 580 Osthoff, H. D., Pilling, M. J., Ravishankara, A. R., and Brown, S. S.: Temperature dependence of the NO₃ absorption cross-section above 298 K and determination of the equilibrium constant for NO₃ + NO₂ <-> N₂O₅ at atmospherically relevant conditions, *Phys. Chem. Chem. Phys.*, 9, 5785-5793, 2007.
- Pilegaard, K.: Processes regulating nitric oxide emissions from soils, *Philos T R Soc B*, 368, ARTN 20130126 10.1098/rstb.2013.0126, 2013.
- 585 Platt, U., Perner, D., Winer, A. M., Harris, G. W., and Pitts, J. N. J.: Detection of NO₃ in the polluted troposphere by differential optical absorption, *GRL*, 7, 89-92, 1980.
- Schuster, G., Labazan, I., and Crowley, J. N.: A cavity ring down / cavity enhanced absorption device for measurement of ambient NO₃ and N₂O₅, *Atmos. Meas. Tech.*, 2, 1-13, 2009.
- 590 Smith, J. P. and Solomon, S.: Atmospheric NO₃. 3. Sunrise Disappearance and the Stratospheric Profile, *J. Geophys. Res. - Atmos.*, 95, 13819-13827, 1990.
- Smith, N., Plane, J. M. C., Nien, C. F., and Solomon, P. A.: Nighttime Radical Chemistry in the San-Joaquin Valley, *Atmos. Env.*, 29, 2887-2897, 1995.
- Sobanski, N., Schuladen, J., Schuster, G., Lelieveld, J., and Crowley, J. N.: A five-channel cavity ring-down spectrometer for the detection of NO₂, NO₃, N₂O₅, total peroxy nitrates and total alkyl nitrates, *Atmos. Meas. Tech.*, 9, 5103-5118, 10.5194/amt-9-5103-2016, 2016.
- 595



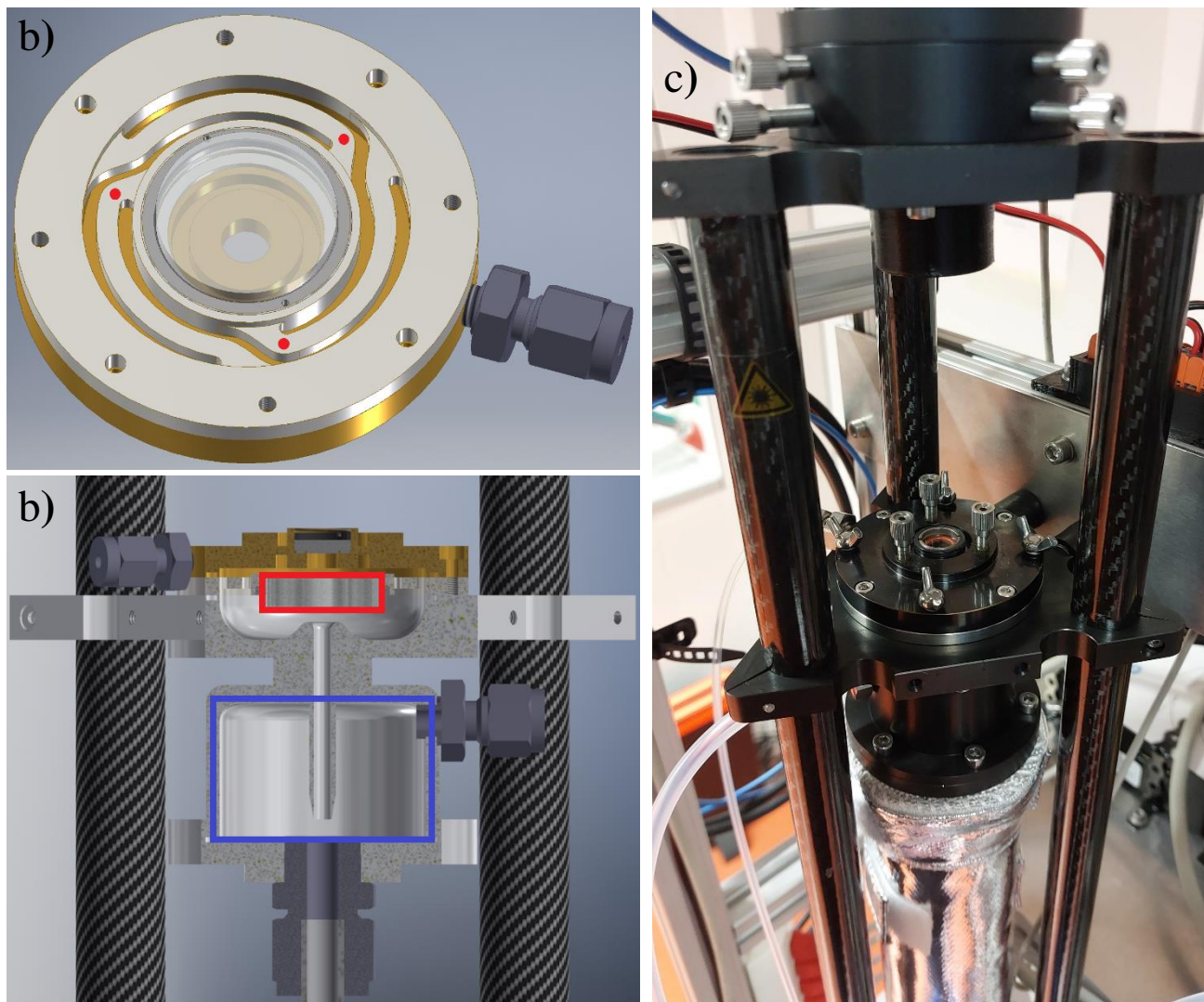
- Stutz, J., Alicke, B., Ackermann, R., Geyer, A., White, A., and Williams, E.: Vertical profiles of NO_3 , N_2O_5 , O_3 , and NO_x in the nocturnal boundary layer: 1. Observations during the Texas Air Quality Study 2000 *J. Geophys. Res. -Atmos.*, 109, art. D12306, 10.1029/2003JD004209, 2004.
- 600 Tang, M. J., Thieser, J., Schuster, G., and Crowley, J. N.: Uptake of NO_3 and N_2O_5 to Saharan dust, ambient urban aerosol and soot: a relative rate study, *Atmos. Chem. Phys.*, 10, 2965-2974, 2010.
- Vandaele, A. C., Hermans, C., Fally, S., Carleer, M., Colin, R., Merienne, M. F., Jenouvrier, A., and Coquart, B.: High-resolution Fourier transform measurement of the NO_2 visible and near-infrared absorption cross sections: Temperature and pressure effects, *J. Geophys. Res. -Atmos.*, 107, Art. 4348, 10.1029/2001JD000971, 2002.
- 605 Voigt, S., Orphal, J., Bogumil, K., and Burrows, J. P.: The temperature dependence (203-293 K) of the absorption cross sections of O_3 in the 230-850 nm region measured by Fourier-transform spectroscopy, *J. Photochem. Photobiol. A-Chem.*, 143, 1-9, 2001.
- von Friedeburg, C., Wagner, T., Geyer, A., Kaiser, N., Vogel, B., Vogel, H., and Platt, U.: Derivation of tropospheric NO_3 profiles using off-axis differential optical absorption spectroscopy measurements during sunrise and comparison with simulations, *J. Geophys. Res. -Atmos.*, 107, 10.1029/2001JD000481, 2002.
- 610 Wagner, N. L., Dube, W. P., Washenfelder, R. A., Young, C. J., Pollack, I. B., Ryerson, T. B., and Brown, S. S.: Diode laser-based cavity ring-down instrument for NO_3 , N_2O_5 , NO , NO_2 and O_3 from aircraft, *Atmos. Meas. Tech.*, 4, 1227-1240, 10.5194/amt-4-1227-2011, 2011.
- Wagner, T., Otten, C., Pfeilsticker, K., Pundt, I., and Platt, U.: DOAS moonlight observation of atmospheric NO_3 in the Arctic winter, *Geophys. Res. Lett.*, 27, 3441-3444, <https://doi.org/10.1029/1999GL011153>, 2000.
- 615 Wayne, R. P., Barnes, I., Biggs, P., Burrows, J. P., Canosa-Mas, C. E., Hjorth, J., Le Bras, G., Moortgat, G. K., Perner, D., Poulet, G., Restelli, G., and Sidebottom, H.: The nitrate radical: Physics, chemistry, and the atmosphere, *Atmos. Env. A*, 25A, 1-206, 1991.



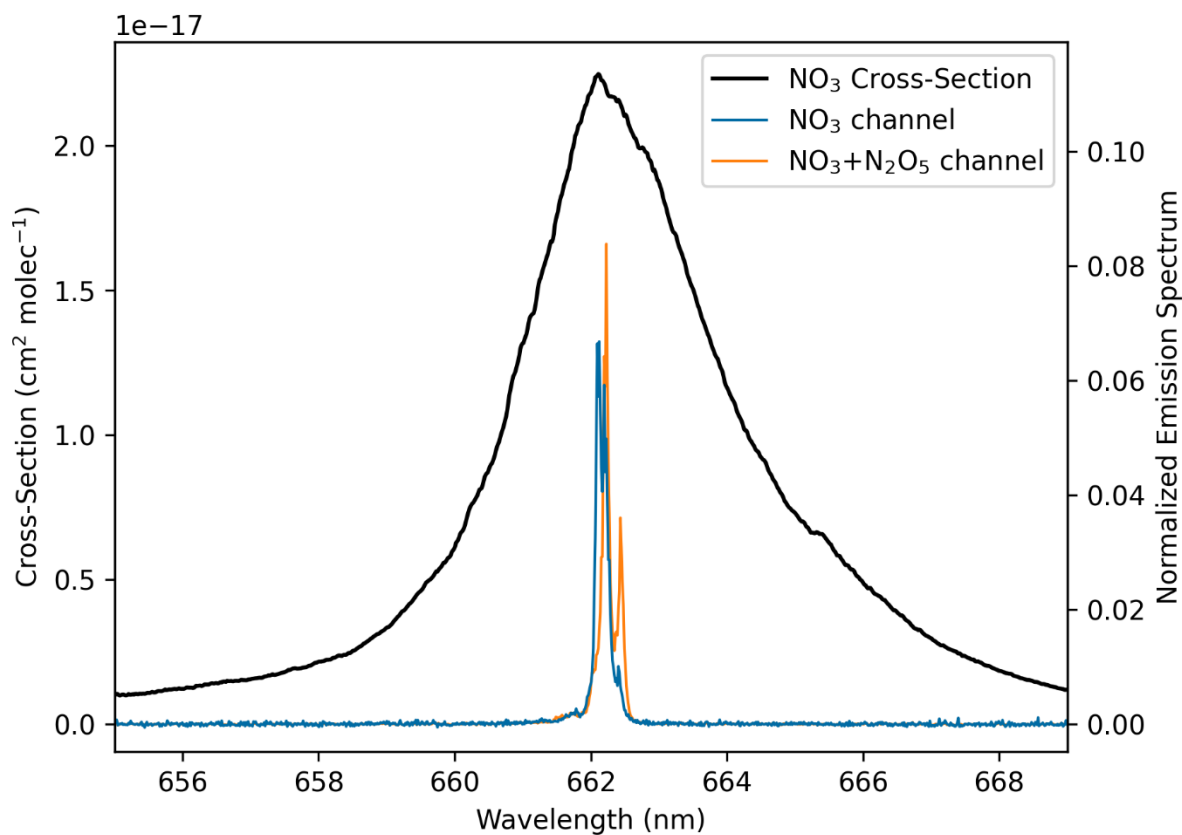
620 **Figures and Tables:**



625 **Figure 1:** A schematic drawing of the 2CH-CRDS instrument. Ambient air is sampled through an automatic filter changer, after which NO can be added for zero measurement (i.e. of τ_0). The left-hand cavity measures $[\text{NO}_3]$ at room temperature, the air in the right-hand channel passes a heating unit set to 443K, ensuring the thermal dissociation of N_2O_5 to measure the sum of $\text{NO}_3 + \text{N}_2\text{O}_5$ in the cavity at 373 K. The walls of the filter changer and the T-shaped glass pieces are FEP-coated, while every other surface is made from PFA. The mirror chambers and connected mixing chamber are made from anodized aluminium.



630 **Figure 2:** a) Technical drawing of the newly designed mirror mount. Three fine adjustment screws control the tilt
of the mirror by applying pressure from behind at the locations indicated by red dots. b) A semi-half section of the
mirror mounting assembly shows the completely sealed mirror (red border) within a separated chamber, which is
flushed with purge gas / zero air. As depicted in Figure 1, the purge gas is then injected into the mixing chamber
(indigo border) while sampled air enters from below. The mixed air then exits through the PFA connector on the
635 right. c) A photo of the mirror mount assembly within the instrument shows the screws for mirror adjustment and
wing screws for easy removal when cleaning is required. Triangle-shaped adapter plates are used to mount the
individual optical elements, while carbon fibre-reinforced polymer tubes create the main frame of each channel.



640 **Figure 3:** The laser emission spectra for both channels (orange and blue) normalized to unit area. The NO₃ absorption cross-sections (black) as reported by Orphal et al. (2003) at room temperature and rescaled to the recommended value by Iupac (2025).

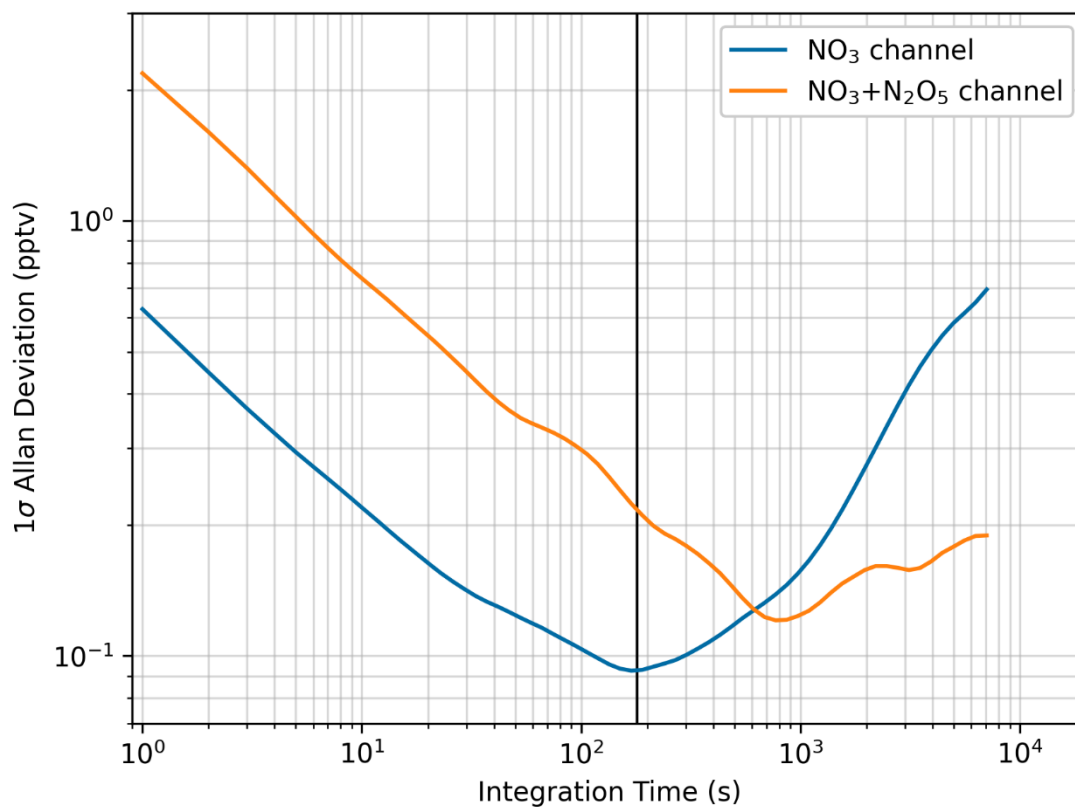


Figure 4: Allan Deviation plots for both cavities based on 1 s data. The integration time of 3 minutes is indicated by the black vertical line. The data were recorded while measuring zero air over a period of 6 hours at night under laboratory conditions.

645

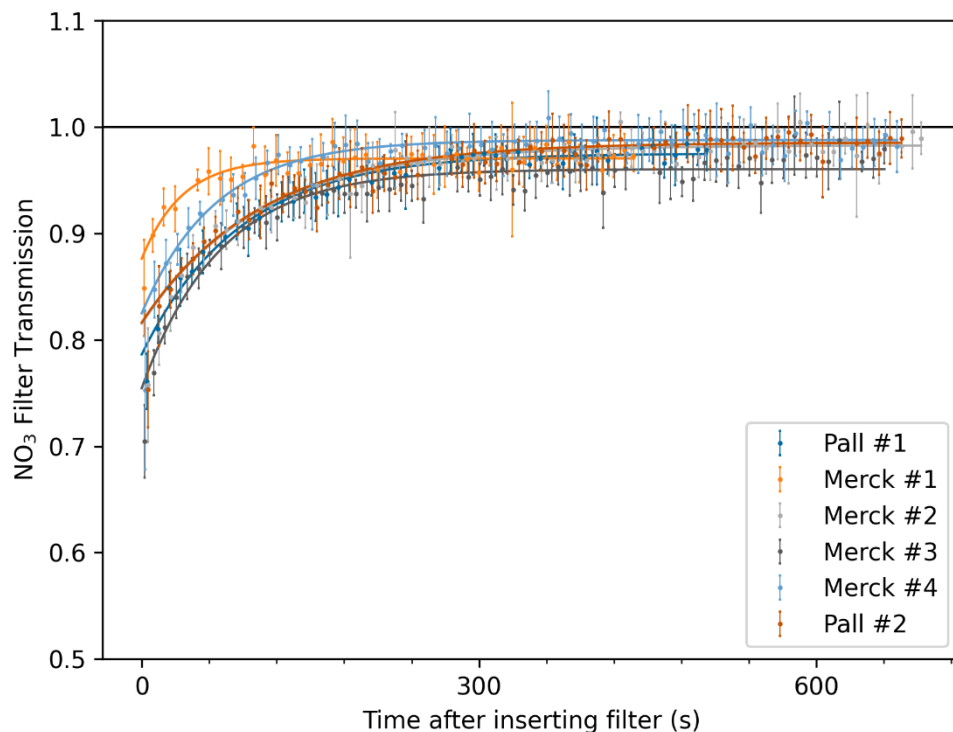


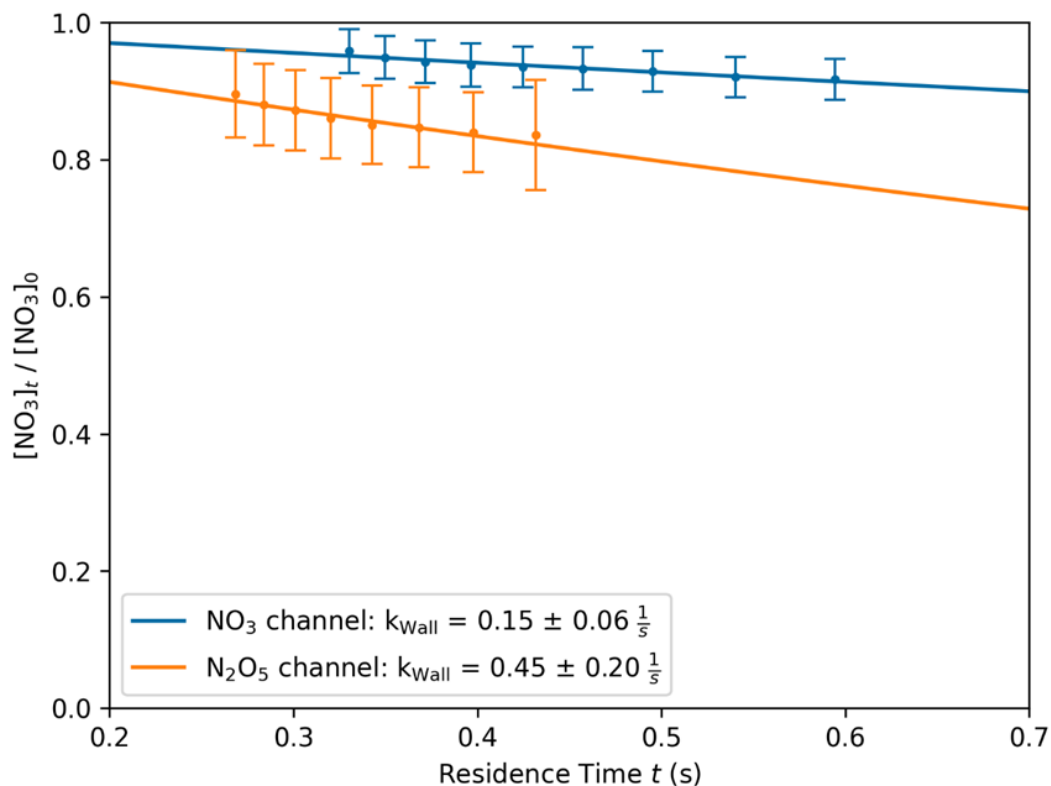
Figure 5: NO₃ transmission measurements for different PTFE filters. The error bars are the statistical uncertainty (2σ) based on averaging for 10 s. Equation (3) was used to derive the maximum transmission. An overview of all T_{max} can be seen in Table 1, and a similar comparison with filters from Cytiva is shown in Figure S1.



Table 1: Overview of estimated maximum transmission factors for new PTFE filters of different brands.

Label	Manufacturer ID	T_{max} in %
Pall #1	AW15675	97.5 ± 0.8
Merck #1	W20309094	97.1 ± 0.7
Merck #2	W20309097	98.3 ± 0.6
Merck #3	W20309095	96.0 ± 0.6
Merck #4	W20309096	98.8 ± 0.5
Pall #2	AW15680	98.5 ± 0.7
Pall #3	AW15679	101.0 ± 0.5
Cytiva #1	C1898521	95.4 ± 0.6
Cytiva #2	C1898520	98.7 ± 0.7
Cytiva #3	C1898519	98.3 ± 0.5
Cytiva #4	C1898518	100.5 ± 0.9

Notes: The uncertainties of T_{max} are based on the covariances and do not reflect NO_3 source fluctuations.



655

Figure 6: Determination of wall loss rates (k_{Wall}) by variation of the residence times (t) for both channels. The measured values are based on the average and two standard deviations of 3 minutes of data, normalized to the initial value of a mono-exponential fit.

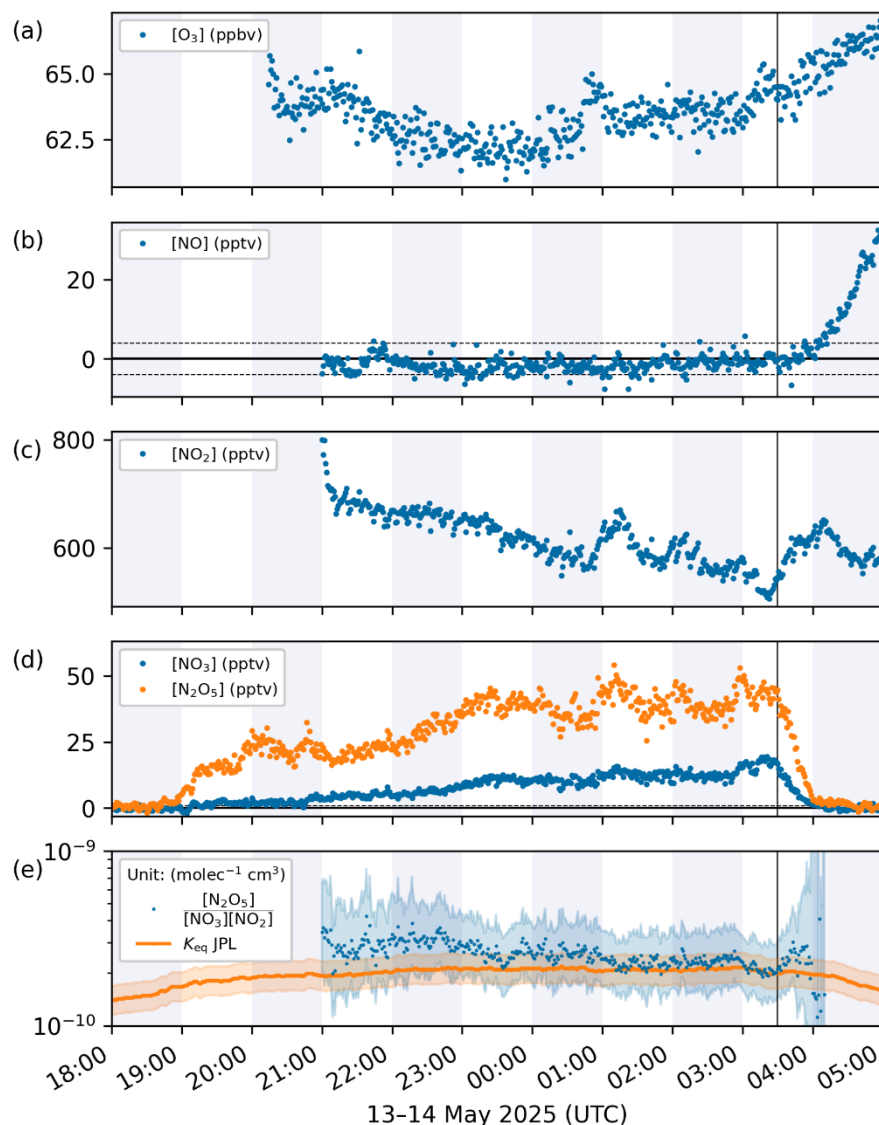
660



Table 2: Overview of channel specific characteristics and uncertainties which significantly influence the total measurement uncertainty (TMU).

Characteristic / Uncertainty		[NO ₃]	[N ₂ O ₅]
NO ₃ absorption cross-section (σ)		(5 %) at 295 K	(8 %) at 373 K
Mirror distance / Absorption path length (R_L)		1.11 ± 0.02 (1.8 %)	1.13 ± 0.06 (5.3 %)
NO + O ₃ during titration		< 0.5 ppt ^a	
Filter changer – NO ₃ transmission (T_{FC})		0.80 ± 0.05 (6.4 %)	–
Clean filter – NO ₃ transmission (T_{Filter})		0.98 ± 0.04 (4.1 %)	–
Wall loss / NO ₃ transmission efficiency	$T_{NO_3, \text{unheated}}$	0.94 ± 0.03 (3.2 %)	
	$T_{NO_3, \text{heated}}$	–	0.86 ± 0.06 (7.0 %)
	$T_{NO_3, \text{heated}}^*$	–	0.90 ± 0.04 (4.8 %)
N ₂ O ₅ transmission ($T_{N_2O_5}$)		–	1.00 ± 0.04 (4.0 %) ^b
Short reaction time of dissociated NO ₃ (C_{dissoc})		–	1.01 ± 0.01 (1.0 %)
Total Measurement Uncertainty		9.8 %	≥ 11.5 % ^c

665 **Notes:** ^a See conditions in Section 3.3 ^b Value taken from Schuster et al. (2009) ^c This value holds for low ambient temperatures when mixing ratios of NO₃ are very low compared to N₂O₅ and increases with the ratio of NO₃/N₂O₅, see Supplement S2. The relative uncertainties of each contribution are shown in brackets.



670 **Figure 7:** Nighttime data from a field campaign in May 2025 at Kleiner Feldberg, Germany. Sunset was at 19 UTC
 while sunrise occurred at 3:30 UTC (vertical black line). (a) Ozone was detected by a commercial UV-absorption
 instrument, while (b) NO and (c) NO₂ were measured by the CLD instrument. Panel (d) presents measurements of
 NO₃ and N₂O₅ by our new 2CH-CRDS instrument, while (e) shows the equilibrium constant K_{eq} (including
 675 uncertainty) based on the measurements of NO₂, NO₃ and N₂O₅ in comparison to the recommended value (incl.
 uncertainty) by JPL (Burkholder et al., 2020), which depends on ambient temperature.